Composites Part C: Open Access 8 (2022) 100244

Contents lists available at ScienceDirect

Composites Part C: Open Access

journal homepage: www.elsevier.com/locate/composites-part-c-open-access

Double–Double laminates for aerospace applications — Finding best laminates for given load sets

Erik Kappel

DLR, Institute of Composite Structures and Adaptive Systems, Lilienthalplatz 7, 38108 Braunschweig, Germany

ARTICLE INFO

Keywords:
Laminate optimization
Double–Double laminates
Light-weight design
Automated manufacturing

ABSTRACT

The Double–Double (DD) family of laminates is characterized by the parametric laminate description $[\pm\varphi, \pm\psi]_{rT}$. DD promises considerable advantages for aerospace laminates, as the unique combination of the laminates' building-block architecture simplifies manufacturing and in particular laminate optimization. DD eliminates complicated permutation issues know from conventional laminates and allows for easy stiffness tailoring, by locally varying repeats r. The present paper proposes a DD-laminate optimization scheme for laminate-strength, which focusses on robustness in the identification of safe laminates. The scheme is presented for a multi-load scenario, each consisting of five individual loads. The combination of the Nettles circle failure enveloped in principle strain with the DD features lead to a rather simple optimization scheme, accompanied by meaningful illustrations, which are presented in the present paper.

1. Introduction

Conventional laminates (CL) in aerospace composite parts are usually composed of $0°, 45°, -45°, 90°$ plies. Various stacking rules or guidelines are applied in practice, as for example the 10% (sometimes 8%) rule, the balance requirement of $\pm$ plies and most-important, the symmetry requirement. Those rules/guidelines were introduced to assure robust laminates, which do not show difficult warpage and twist distortions after manufacturing and in service. However, clear explanations or experimental substantiation, in particular for the pre-definition of ply angles, are lacking.

At the same time, these rules are responsible for the fact that laminate stackings are often non-optimal, leading to unnecessarily heavy CFRP components and severe difficulties in context of laminate optimization.

The present paper focusses on 'Double–Double' laminates. This laminate family has been introduced, promoted and advanced by Steve Tsai, Daniel D. Melo, Aniello Riccio and others [1–5] in recent years. Key facts and advantageous aspects of DD have been outlined recently by Tsai [3].

The present paper presents a closed strategy for finding best DD-laminates for given load sets. The developed procedure is intentionally set up with an inherent conservatism, which can be controlled by selecting individual material-effort (ME) thresholds within optimization procedure as will be shown below. In this paper, a DD laminate consists of a four-ply building block, and a repetition parameter r, leading to the DD-laminate description:

$$[\pm\varphi, \pm\psi]_{rT} \quad , \tag{1}$$

Therein, the index T denotes 'total' laminate, which is in line with [6]. The DD laminate, as considered here, is balanced but not symmetric. φ and ψ are both in the range between zero and ninety degree. Stacking rules and pre-defined ply orientations, as known for CLs, are intentionally not prescribed.

2. Double–double laminates

DD is often investigated with focus on dry-fiber-composites, where a set of $\pm$ layers is considered a single pre-manufactured NCF ply. In the present paper, the DD idea is pursued with focus on conventional UD-prepreg manufacturing, using AFP technology for example. Thus, a DD laminate building block is composed of four UD plies, oriented in $+\varphi, -\varphi, +\psi$ and $-\psi$ degree.

2.1. Theoretical background

The CLT is state of the art in laminate design today. The typical notation

$$\begin{pmatrix} \{N\} \\ \{M\} \end{pmatrix} = \begin{bmatrix} [A] & [B] \\ [B] & [D] \end{bmatrix} \cdot \begin{pmatrix} \{\varepsilon^0\} \\ \{\varkappa\} \end{pmatrix} \tag{2}$$

features the ABD-matrix (see Nettles [6] for an excellent CLT introduction). For a UD-ply-based aerospace laminate, the ABD matrix usually

E-mail address: erik.kappel@dlr.de.

https://doi.org/10.1016/j.jcomc.2022.100244
Received 1 February 2022; Accepted 16 February 2022
Available online 4 March 2022

Abbreviations

AFP	Automated-fiber-placement
CFRP	Carbon-fiber-reinforced-plastics
CL(s)	conventional laminate(s)
CLT	Classical laminate theory
DD	Double–Double
FPF	First-ply-failure
LPF	Last-ply-failure
ME	Material effort
NCF	Non-crimp-fabric
NC	Nettles circle
NC-R	Nettles circle radius
PSCC	Principal-strain-cut-off-circle
UD	Unidirectional ply

looks like

$$ABD = \begin{bmatrix} \bullet & \bullet & & & & & \\ \bullet & \bullet & & & & & \\ & & \bullet & & & & \\ & & & \bullet & \bullet & \bullet & \\ & & & \bullet & \bullet & \bullet & \\ & & & \bullet & \bullet & \bullet & \end{bmatrix} , \tag{3}$$

wherein the • denote positive non-zero entries. Laminate symmetry assures $[B] = 0$, while the balance requirement assures decoupling of extension and shear $A_{16} = A_{26} = 0$. As long UD plies are used, D_{16}, D_{26} coefficients are usually nonzero, always leading to a coupling between bending and twist of those laminates, which tends to diminish for with the increasing number of plies. When isotropic materials are examined, no coupling exists ($D_{16} = D_{26} = 0$), leading to:

$$ABD_{iso} = \begin{bmatrix} \bullet & \bullet & & & & & \\ \bullet & \bullet & & & & & \\ & & \bullet & & & & \\ & & & \bullet & \bullet & 0 & \\ & & & \bullet & \bullet & 0 & \\ & & & 0 & 0 & \bullet & \end{bmatrix} . \tag{4}$$

One can find

$$\frac{[A]}{t_{lam}} = \frac{[D]}{t_{lam}^3/12} , \tag{5}$$

which is utilized in the following. For DD laminates one can observe the following

$$ABD_{DD} = \begin{bmatrix} \bullet & \bullet & & f(1/r) & f(1/r) & f(1/r) \\ \bullet & \bullet & & f(1/r) & f(1/r) & f(1/r) \\ & & \bullet & f(1/r) & f(1/r) & f(1/r) \\ f(1/r) & f(1/r) & f(1/r) & \bullet & \bullet & f(1/r^2) \\ f(1/r) & f(1/r) & f(1/r) & \bullet & \bullet & f(1/r^2) \\ f(1/r) & f(1/r) & f(1/r) & f(1/r^2) & f(1/r^2) & \bullet \end{bmatrix} , \tag{6}$$

which indicates the remarkable key feature. It is found that the coupling matrix $[B]$ and coupling terms in $[D]$ diminish for increasing number of repeats r, with $1/r$ and $1/r^2$ respectively. This is denoted as homogenization, as

$$\lim_{r\to\infty} \left(\frac{[A]}{t_{lam}} - \frac{[D]}{t_{lam}^3/12} \right) = [0] \tag{7}$$

and

$$\lim_{r\to\infty} ([B]) = [0] . \tag{8}$$

Fig. 1. Flat DD laminate demonstrator, showing no warpage, while the number of repeats is increased locally from $r = 3$ to $r = 10$, leading to laminate thicknesses between 1.5 mm and 5.0 mm with the low-grade prepreg used.

, which is equivalent to the fact that unwanted coupling effects, diminish with the increase of building block repetitions.

Homogenization is key topic in context of DD. Thus, a notation proposed by Tsai and Melo [1] is adopted in this paper, which is:

$$\begin{pmatrix} \{\sigma^0\} \\ \{\sigma^f\} \end{pmatrix} = \begin{bmatrix} [A^*] & [B^*] \\ 3[B^*] & [D^*] \end{bmatrix} \cdot \begin{pmatrix} \{\varepsilon^0\} \\ \{\varepsilon^f\} \end{pmatrix} . \tag{9}$$

This notation utilizes normalized matrices, which are defined as $[A^*] = \frac{1}{h} \cdot [A]$, $[B^*] = \frac{2}{h^2} \cdot [B]$, $[D^*] = \frac{12}{h^3} \cdot [D]$, while h refers to the laminate thickness. Contrary to the CLT, $[A^*], [B^*]$ and $[D^*]$ have the same unit (GPa), while Eq. (5) transfers to $[A^*] = [D^*]$ for a homogenized laminate. As the DD concept adjusts laminate stiffness by defining the appropriate number of repeats, it is observed that the nonzero entries in the normalized matrices are independent from r. Only entries highlighted in Eq. (6) show an r-dependency. Thus, the Young's modulus, for example, remains constant for a DD laminate, independent from the number of repeats.

2.2. A comment on manufacturing DD laminates

The homogenization procedure directly depends on the number of repeats r, where $[B] = f(1/r)$, while D_{16} and $D_{26} = f(1/r^2)$. A minimum number of building-block repetitions of 3 to 4 (better 5 to 6) is mandatory/recommended (see also [3]), to minimize drawbacks related to asymmetric laminate stackings, in particular severe warpage and twist after manufacturing. With the four-ply building block, this recommendation leads to feasible minimum ($r = 3$) laminate thickness of $4 \cdot r$ plies, which is equivalent to 1.5 mm laminate thickness, when a typical low-grade-prepreg ply thickness of $t_{ply} = 0.125$ mm is adopted. Thus, increasing the number of repetitions is beneficial for DD laminates, which explains that DD is often discussed in context with thin-ply approaches, using plies with low fiber-area weights, as for example 50 g/m^2. However, as shown with the demonstrator in Fig. 1, which is made from conventional low-grade prepreg ($t_{ply} = 0.125$ mm), DD also works with conventional prepregs. It is highlighted that for DD, laminate-thickness changes are realized by drop-offs of complete building-blocks (4-plies at once).

Contrary to CLs, those drop-offs can be located on either the bag-sided or the tool-sided surface of the part, which minimizes fiber undulations and the amount of resin-rich areas (resin pockets), in the inner laminate architecture. Fig. 1 shows a laminate with drop-offs-located on the bag-side (top-surface) of the panel. Due to the omission of the CLs' symmetry requirements, local thickness changes become easy in DD laminates, as the additional plies do not need to be distributed within the laminate stack.

2.3. DD-replacements for CL

Finding DD replacements to substitute CLs is possible[1] for most cases, as outlined by Tsai [3]. The finding procedure, however, can

[1] It has been shown that DD substitutes for CLs can be identified, either on basis of $[A^*]$, $[D^*]$ or both. However, when a more-orthotropic conventional

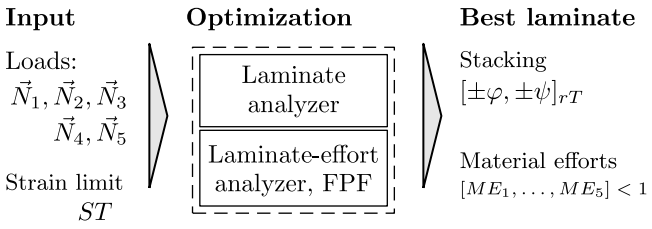

Fig. 2. Principle architecture of the procedure.

be set up in different ways, while the most suited strategy depends on the laminate's load case in focus. The procedure can focus on $[A^*]$ or $[D^*]$ (in-plane or flexure properties) or a simultaneous consideration of both. DD replacements can be determined for single laminates, but they can also be determined for laminate groups. The latter approach leads to a kind of averaged laminate, as an example of a fuselage shell shows [1]. It is found that the best DD replacement for a group of laminate stackings is very close to the averaged properties of the individual laminates in the group. Identifying a DD laminate, which is the best replacement for a set of individual CLs, is related to the particular opportunities provided by the DD laminate family, when locally varying laminate stiffness ($\propto [A^*] \cdot t_{lam}$) is realized by locally adapting the number of repeats.

It is highlighted here that mimicking a CL with a DD is usually possible. However, a CL imitation is a replacement with similar (up to identical) stiffness properties, which usually will not lead to remarkable advantages in terms of laminate working stress at failure. The full DD potential becomes accessible, when one does not try to mimic CLs. Instead, it is the approach (pursued in this paper) to determine the best combination of φ, ψ and r for a given set of loads, without limiting constraints coming from stacking rules or other detrimental boundaries. Fig. 2 shows the general procedure presented in this paper, which is completely realized in Python.

The illustrated 'Laminate analyzer' is a rather simple routine, which basically returns $[A^*], [B^*]$ and $[D^*]$ matrices, as a function of the stacking sequence, Engineering constants of the UD ply and the ply thickness. The 'Laminate-effort analyzer' requires additional attention. Thus, it is explained in detail within the following section.

3. Omni FPF envelope in strain space

Assessing laminate failure is a key element in the present paper, as indicated in Fig. 2. Laminate failure is often analyzed ply wise, wherein ply loads are assessed in the plies' on-axis (local) coordinate system. In this paper a laminate wise failure assessment strategy is pursued, as it is considered to significantly simplify the design process. The following analyses base on the quadratic failure criterion in stress-space [1, p. 221], which is also the basis for well known failure criteria as Tsai–Hill, Hoffmann and Tsai–Wu. The stress-space criterion is transferred into strain space here, by using

$$F_{ij}\sigma_i\sigma_j = [F_{ij}Q_{ik}Q_{kl}]\varepsilon_k\varepsilon_l = G_{kl}\varepsilon_k\varepsilon_l \tag{10}$$

$$F_{ij}\sigma_i = [F_iQ_{ij}]\varepsilon_j = G_j\varepsilon_j \quad . \tag{11}$$

Thus, the scalar equation in strain-space becomes:

$$G_{ij}\varepsilon_i\varepsilon_j + G_i\varepsilon_i = 1 \tag{12}$$

In order to use the criterion for assessing laminates' first-ply-failure (FPF), one advantage of the strain-space criterion is essential. The strain-space criterion allows for assessing failure with respect to arbitrary coordinate systems. The corresponding transfer from the on-axis to off-axis orientation is described in [1, p. 243]. Thus, failure of differently oriented plies in the laminate are assessed with respect to a common orientation, the global laminate orientation.

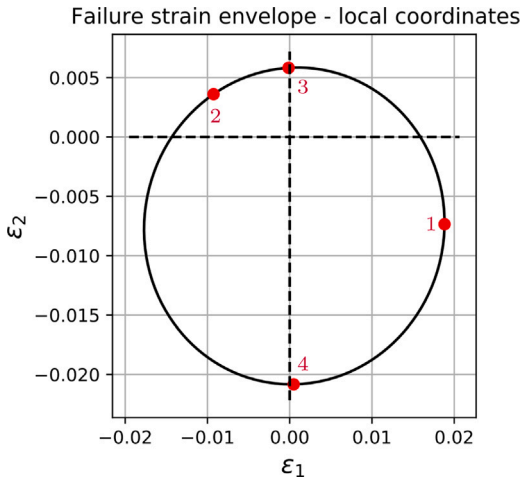

Fig. 3. Strain-space failure envelope for M21E/IMA UD prepreg, with red anchor points determined from conventional ply-strength values. (Data provided in Tables 1–3).

Table 1
Strain-space failure envelope anchor points. Shear anchor is not shown.

Anchor	ε_1	ε_2
1	X/E_1	$-\nu_{12}\cdot\varepsilon_1$
2	$-X'/E_1$	$-\nu_{12}\cdot\varepsilon_1$
3	$-\nu_{12}\cdot\frac{E_2}{E_1}\cdot\varepsilon_2$	Y/E_2
4	$-\nu_{12}\cdot\frac{E_2}{E_1}\cdot\varepsilon_2$	$-Y'/E_2$

3.1. Strain-space failure envelope for UD ply

The strain-space failure envelope ($\varepsilon_1 - \varepsilon_2$ plane shown) is the basis for determining the laminate FPF envelope. Fig. 3 shows the ply's envelope for Hexcel's M21E/IMA carbon fiber epoxy prepreg, determined from the data provided in the Tables 2 and 3.

The envelope characterizes the UD-ply failure, for the Tsai–Wu criterion with $F^*_{12} = -0.5$. Note, that this selection represents no limit of the concept. The illustrated anchor points are determined from regular strength parameters by using the equation provided in Table 1.

3.2. Laminate omni-failure envelope

In order to assess laminate failure, instead of single ply failure, one has to describe the failure characteristics of the specific plies with respect to a common coordinate system, the laminate coordinate system.

The G_{ij} and G_i parameters depend on the F_{ij} parameters and on Q_{ij}, which both change with the ply-angle-specific rotation, as described in [1, p. 243].

In order to capture failure of all conceivable ply orientation in the laminate, the failure envelopes of all plies are transferred in a common coordinate system. Note that the procedure is illustrated here in 2D, for the zero shear plane. Fig. 4 shows the resulting failure envelopes (zero shear level) for all conceivable full-degree ply orientations between 0° and 90° degree and a more discrete version with only seven equidistant orientations, with respect to the global laminate coordinate system. The colored envelopes are denoted as omni-strain envelopes [3]. Once they have been determined, failure analysis can be executed laminate wise.

laminate is examined, with ply-orientation fractions of 45% of 0° plies in the laminate and above, the match between DD and CL starts getting poorer, which can be explained with the DD laminate characteristics.

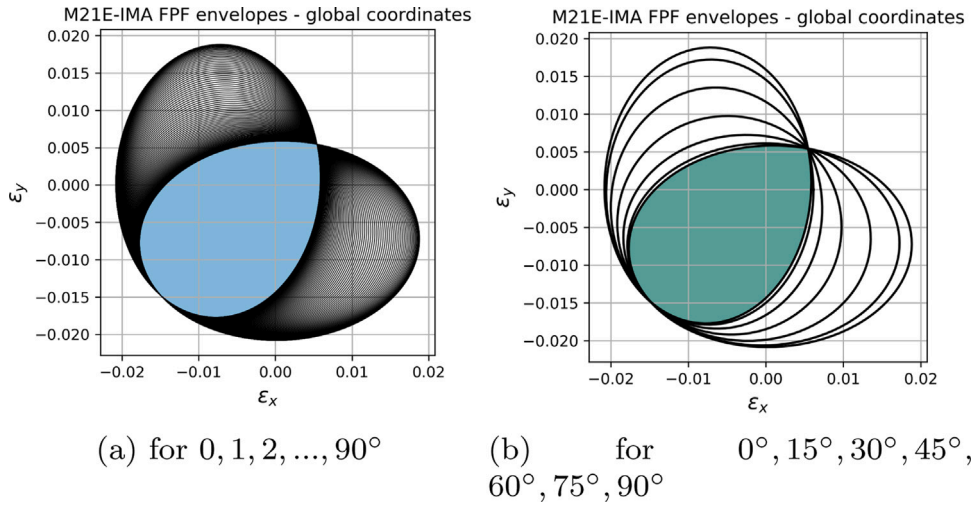

(a) for $0, 1, 2, ..., 90°$ (b) for $0°, 15°, 30°, 45°, 60°, 75°, 90°$

Fig. 4. M21E/IMA laminate strain-space omni failure envelopes.

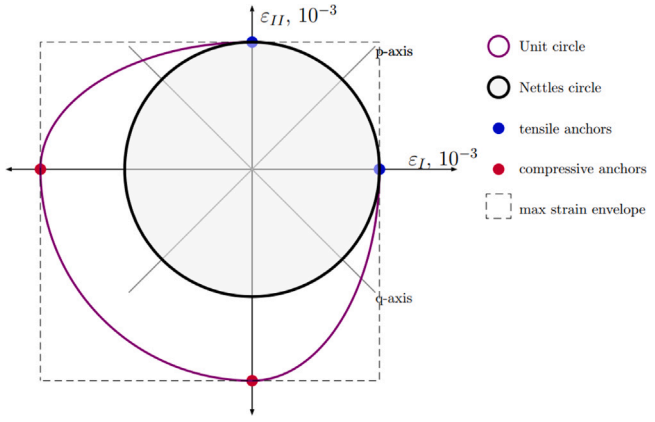

Fig. 5. Example from [3]. Principle strains with tensile anchors at $6.2 \cdot 10^{-3}$ and compressive anchors at $-10.3 \cdot 10^{-3}$.

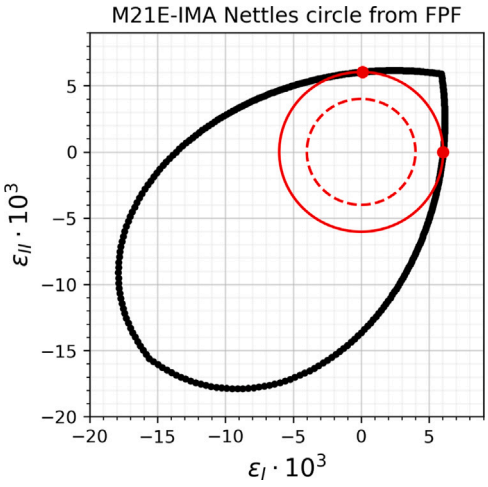

Fig. 6. NC defined based on tension anchors of the FPF envelope. For M21E/IMA, 6034 microstrain are obtained (red solid NC) from Engineering constants and UD ply strength data, while the 4000 microstrain threshold is shown as a dashed red line.

As long a laminate's strain state is within the colored envelope it is considered as a safe laminate.

However, the previous assessment is still difficult as the strain-state needs to be examined in a 3D space, as in-plane and shear strains act. In order to simplify the procedure further, the strains are transferred to principle strains

$$\varepsilon_x, \varepsilon_y, \gamma_{xy} \rightarrow \varepsilon_I, \varepsilon_{II} \quad , \tag{13}$$

which transfers the failure-assessment problem to the 2D level, as shear strains diminish. The transfer is executed using Mohr's circle in strain space, while the principle strains are determined with.

$$\varepsilon_{I,II} = \frac{\varepsilon_x + \varepsilon_y}{2} \pm \sqrt{\left(\frac{\varepsilon_x - \varepsilon_y}{2}\right)^2 + \left(\frac{\gamma_{xy}}{2}\right)^2} \quad . \tag{14}$$

3.3. PSCC or Nettles circle

The description of laminate principle strains allow for assessing FPF and also LPF [7], while the latter requires an additional analysis step with drastically degraded resin properties. When FPF analysis is complemented with an LPF analysis, the unit-circle laminate failure envelope can be defined [7], which features four characteristic anchor points. Both tension anchors and both compression anchors are connected with individual circular arcs, while the mixed domains are connected with elliptical arcs, as shown in Fig. 5.

FPF analysis represents the most conservative approach. It assures, on a theoretical basis, that all plies stay intact, which is in line with the ambition of the present paper. Thus, a simplified configuration of the unit-circle criterion is pursued here, which describes the full envelope based on the tensile anchors only, leading to a circular-shape envelope in all strain domains. Thus, the envelope is fully characterized by a single radius, which represents the principle-strain magnitude threshold. This particular form of the unit-circle envelope can be described as a PSCC while it is also known as Nettles circle (NC) [3].[2]

Fig. 6 shows the FPF envelope for M21E/IMA and the corresponding NC (red-solid line). The plot shows another circle as a red dashed line, which illustrates an optional, conservative feature of the presented procedure. The NC is directly determined based on the ply data. The dashed circle represents a self-defined strain threshold (ST), which can be defined based on experience and/or based on company-specific prescriptions for example. In the following section NCs for selected carbon-fiber epoxy materials are presented.

[2] It should be noted that the anchor points can be used to define the Max-strain criterion in principle strains as well.

Table 2
UD ply Engineering constants and sources. Entry marked with * is taken from [9].

Material	E_1 GPa	E_2 GPa	ν_{12} –	G_{12} GPa
8552/AS4 [10]	141.0	9.75	0.267	5.20
M21E/IMA [11]	160.8	9.30	0.340	5.20*
T800H/3900-2 [12]	152.4	9.20	0.350	4.30
IM7/977-3 [2]	191.0	9.94	0.350	7.79
T300/976 [13]	133.7	9.24	0.318	6.27

Table 3
Strength values in MPa and sources.

Material	X	X'	Y	Y'	S
8552/AS4 [10]	2200	1500	81	260	80
M21E/IMA [11]	3050	1500	56	200	95
T800H/3900-2 [12]	2089	1482	79	231	133
IM7/977-3 [2]	3250	1600	62	98	75
T300/976 [13]	1427	1505	39	206	76

Table 4
NC-R for examined materials in Microstrain.

Material	NC-R
8552/AS4	8337
M21E/IMA	6034
T800H/3900–2	8616
IM7/977–3	6253
T300/976	4202

3.4. Example materials

Two important statements from the literature are recalled here, as those where utilized in the following to define the radius of the dashed NC. The first statement is *'Nearly all composite structures for aerospace have been built with a strain cutoff at 4000 microstrain as a circle. With this strain cutoff, damage tolerance of laminates against impact is sufficiently assured'* is given in Tsai's [3] recent paper on DD laminates. The second statement: *'Typical maximum strain values used in design are between 4000–5000 microstrain (strain $\times 10^6$) in tension and 3000–4000 microstrain in compression'*, can be found in Baker [8]. As robustness and also the safe selection of best laminates is in focus of the present paper. Hence, the laminate-strain threshold of 4000 microstrain is incorporated in the plots shown hereafter (see [1, p. 243]). Its presence eases the direct comparison of the material-specific laminate capabilities. The selection of 4000 microstrain is again no limitation for the concept.

The provided Engineering constants (Table 2) and the strength data (Table 3) are utilized to determine the Nettles-circle representations, which are shown in Fig. 7.

The inherent conservatism of the concept becomes obvious when comparing the full FPF envelope, which already represents the laminate's 'safe region' and the corresponding NCs. With respect to the two aforementioned statements, the graphs clearly show that a strain threshold of 4000 microstrain is well within the strength-value-based NCs (see Table 4), with radii (NC-R) values found between 4202 and 8616 microstrain for the individual materials. However, for T300/976, the difference is already rather small, which is a consequence of the particularly low tensile strength values for this material (see Table 3).

The NC approach is pursued here, as it is expected to provide robust conservative laminate solutions, which are usually desired for aerospace applications. If close-to-the-edge solutions are of interest, the FPF + LPF envelopes can be directly used (see [3]), while principle-strain-states close to the envelope's edge promise the lightest structures.

Table 5
Loads Ni for the three different scenarios. Normal and shear forces N_i are given in MN/m.

		N1	N2	N3	N4	N5
Fuselage	N_x	0.5	0.5	0.5	0	−0.1
	N_y	1	1	−0.1	1	1
	N_{xy}	0	0.2	0.2	0.2	0.2
Upper Wing	N_x	−1	−1	−1	0.2	0.5
	N_y	0	0.2	0.2	−0.4	0
	N_{xy}	0	0	−0.3	0	0
Lower wing	N_x	1	1	1	0.2	0.5
	N_y	0	0	−0.2	−0.4	0
	N_{xy}	0	0.3	0.3	0	0

4. Finding best DD laminates

In this section it is demonstrated how 'best' DD laminates are identified for three different load collectives, each consisting of five individual loads. The study is focussed on Hexcel's M21E/IMA UD prepreg. The examined load cases are provided in Table 5. They are clustered in the three categories fuselage, upper wing and lower wing.[3]

An optimization framework has been set up for the task at hand, as shown in Fig. 2. Essential steps within the procedure are the determination of global laminate strains according to

$$\begin{Bmatrix} \epsilon_x \\ \epsilon_y \\ \gamma_{xy} \end{Bmatrix} = \frac{1}{t_{lam}} \cdot [A^*]^{-1} \cdot \begin{Bmatrix} N_x \\ N_y \\ N_{xy} \end{Bmatrix} \quad , \tag{15}$$

while $[A^*]$ depends on the ply orientations and repeats $f([\pm\varphi, \pm\psi]_{rT})$. The $[A^*]$ and its inverse is determined within the 'Laminate analyzer' routine, which is basically an adapted CLT routine. In line with the NC concept, the principal laminate strains are calculated according to the relations of Mohr's circle in strain space, provided in Eq. (14). Therefore, the laminates' material effort is defined as the principle-strain magnitude divided by the considered strain threshold (ST), leading to:

$$ME_i = \frac{\sqrt{\varepsilon_{I,i}^2 + \varepsilon_{II,i}^2}}{ST} \quad . \tag{16}$$

As multiple loads are examined here, the index i indicates the relation to the ith load in the set. Thus, five ME-values are determined for a specific laminate configuration. A laminate belongs to the group of feasible solutions as long all five ME values are ≤ 1, while the strain threshold can be defined by the user as outlined above.

4.1. Optimization

The problem is approached as an optimization scenario. The results presented in this paper are determined with MIDACO [15] utilized in a Python-based framework. Alternative algorithms can likely be used, but were not in focus of the present study. The optimization problem at hand is described by the following key points:

- Optimization parameters: Integer values for ply orientations[4] and repeats $\vec{x} = [\varphi, \psi, r]$,
- Design space:
  - Repeats: $1 \leq r \leq 10$

[3] The load were discussed with Prof. Steve Tsai and they were also presented in [14].

[4] Full-degree ply angles are considered a reasonable limitation driven by realistic manufacturing boundaries, coming from AFP machines for example. There is no limitation related to MIDACO.

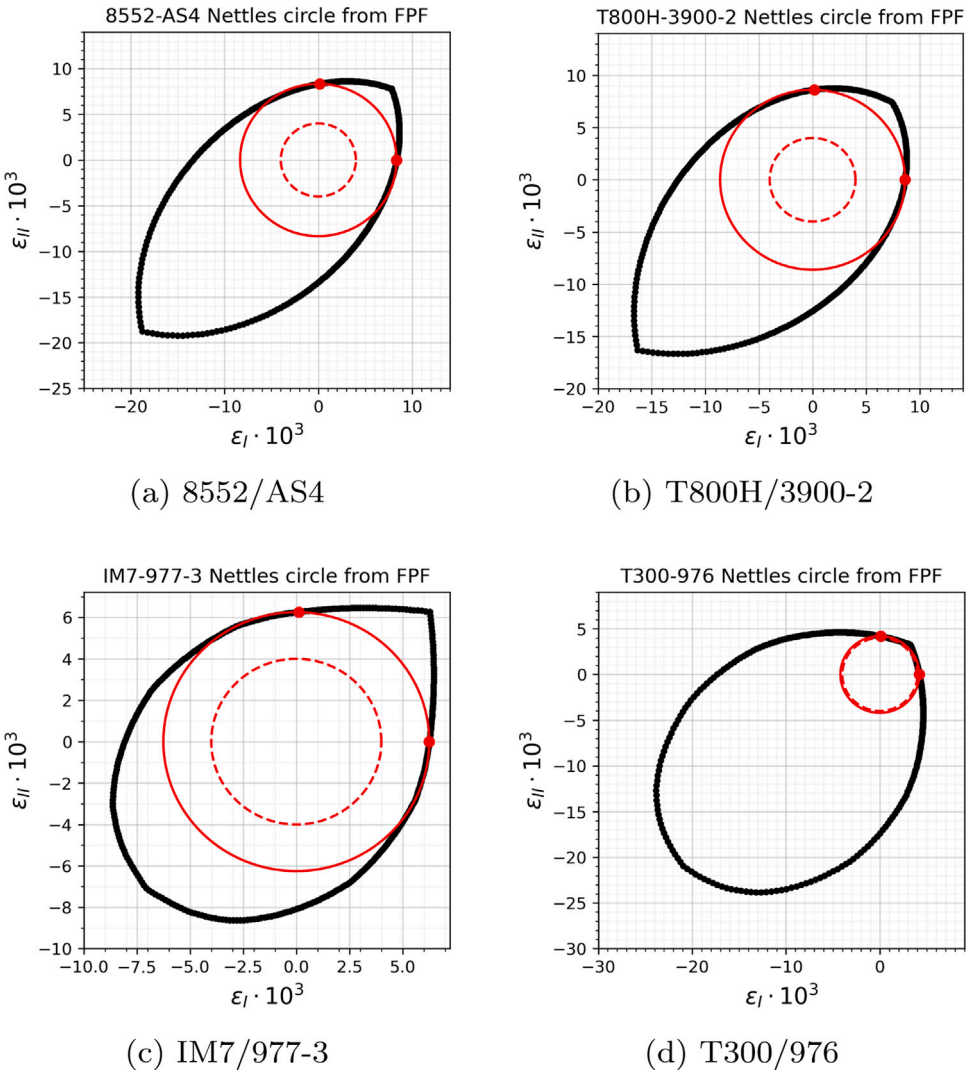

Fig. 7. Nettles-circles for various materials from Table 2. The dashed red circle represent the selected 4000 microstrain limit.

  - Ply angles $0° \leq \varphi, \psi \leq 90°$

- Objectives:
  1. Minimize repeats r (minimum weight)
  2. Minimize material effort $\sum_i ME_i$ (Highest load-increase capacity)

- Inequality constraints to assure being inside NC for all loads: $g_i: \quad -(ME_i - 1) \overset{!}{\geq} 0$
- Best result: Solution for the control load, with minimum ME

It should be noted that both objectives have competing character. Minimizing r leads to an increase of the material effort as the laminate thickness reduces. Minimizing the material effort leads to an increase of repeats, which is equivalent to an increasing laminate thickness. To overcome this challenge, a two step procedure has been executed here.

In the first step the full group of feasible solutions, which is determined for a wide range of the r parameter, (e.g. between 1 and 10) is examined. In the subsequent step, the group is subdivided based on the identified r-levels, while the group with the lowest r-level is of particular interest, as it refers to the lightest laminates. For example, a sub group is identified, which represents feasible solutions for six building-block repeats. In a second run, the r-parameter is then limited to $r = 6$, which in fact represents a reduction of the design space and also a change to a single objective formulation, leading to the ply-angle combination which shows the lowest ME value, within the sub-group of the lightest feasible solutions.

Fig. 8 shows the determined solutions for the three examined load sets (see Table 5). A strain threshold of 4000 microstrain has been used within the analysis. For each load case, the feasible solutions are plotted for the full design space (left plots). The plots on the right refer to the sub-group with minimum repeats.

The colored circles refer to the load-specific strain states, which allows the direct visual identification of the dominating load case, when the solutions closest to the NC's edge are picked.

The fuselage example outlines the procedure. For the full design space, feasible solutions are identified which are rather close to the center of the NC. Those solutions are characterized by little ME values, which indicates too heavy laminates. For the fuselage example, a minimum of eight building-block repeats is determined necessary to sustain all loads of the fuselage load set. Fig. 8(a) shows the solutions for all feasible laminates with eight repeats. It can be seen that load N5

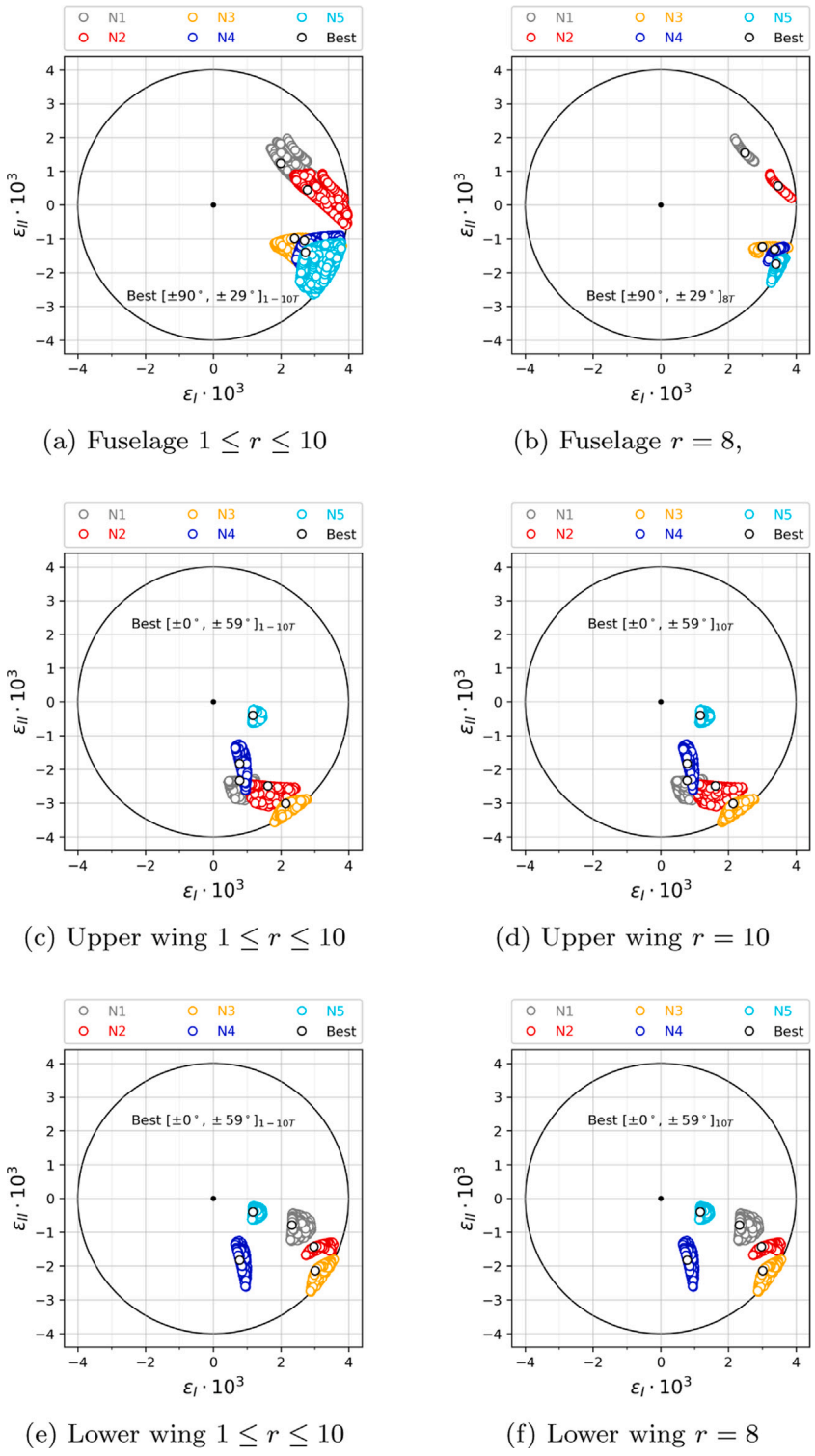

Fig. 8. Results for fuselage, upper wing and lower wing load set with a considered NC-R of 4000 microstrain, illustrated with black solid line. Black-edge circles refer to the identified 'best' solution.

is the dominating load for the fuselage case (sometimes also denoted as control load).

The upper and lower wing configurations show similar results, which becomes obvious when the load-sets are compared. A minimum of ten repeats are identified for both cases, which represents the upper threshold of the examined design-space for the parameter r. For both cases Load N3 is dominating, which leads to identical ply-angles for the identified DD laminates.

Table 6 summarizes the ME values for the examined scenarios with the specific loads. For the minimum r-values configurations, MEs of 95.5%, 92.2% and 92.2% are determined for the fuselage, the lower and the upper wing cover, respectively.

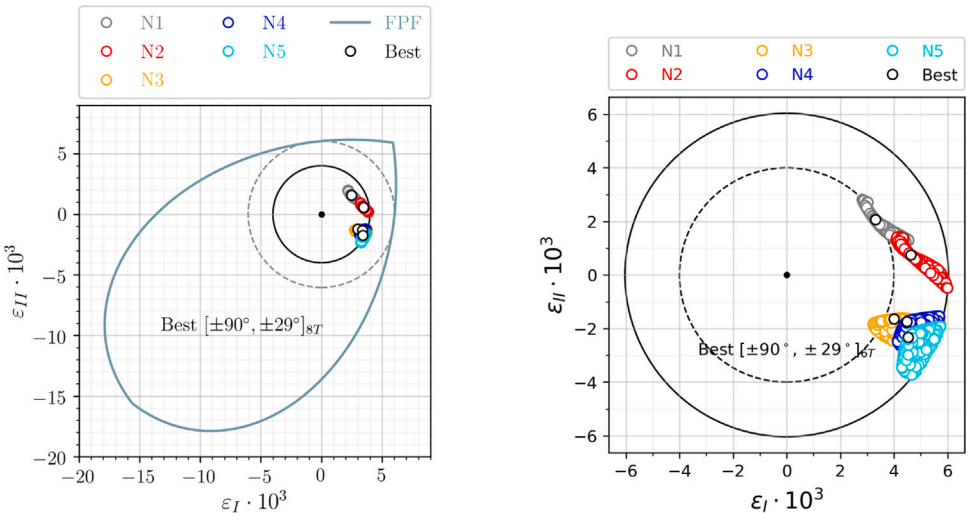

(a) Fuselage $r = 8$ + FPF (b) Fuselage $r = 6$

Fig. 9. Results for the fuselage use-case with the NC-R value of 6043 microstrain from FPF analysis.

Table 6
Load cases Ni for different scenarios. Forces N_i given in MN/m.

	Configuration	ME1	ME2	ME3	ME4	ME5
Fuselage	$[\pm 90, \pm 29]_{1-10T}$	58.6%	70.3%	64.9%	72.1%	76.4%
	$[\pm 90, \pm 29]_{8T}$	73.2%	87.9%	81.2%	90.2%	95.5%
Upper Wing	$[\pm 0, \pm 59]_{1-10T}$	61.3%	73.9%	92.2%	49.4%	30.6%
	$[\pm 0, \pm 59]_{10T}$	61.3%	73.9%	92.2%	49.4%	30.6%
Lower wing	$[\pm 0, \pm 59]_{1-10T}$	61.3%	82.4%	92.2%	49.4%	30.6%
	$[\pm 0, \pm 59]_{10T}$	61.3%	82.4%	92.2%	49.4%	30.6%

Table 7
Loads in MN/m from Sprengholz et al. [13].

	N1	N2	N3	N4	N5
N_x	0.5	−0.05	0	0.1	−0.001
N_y	0.2	−0.05	0	0	0
N_{xy}	0	0	0.001	0.01	0.01

Table 8
Laminate principle strains for optima.

Load case	Layup	ε_I	ε_{II}	$\sqrt{\varepsilon_I^2 + \varepsilon_{II}^2}/Nettles$
N1 - control	$[\pm 31, \pm 32]_{3T}$	3.6724	1.9530	98.9%
N2 - control	$[\pm 31, \pm 32]_{3T}$	0.1425	−1.7627	42.1%
N3 - control	$[\pm 31, \pm 32]_{3T}$	0.0117	−0.0117	0.4%
N4 - control	$[\pm 31, \pm 32]_{3T}$	1.4186	−1.7037	52.7%
N5 - control	$[\pm 31, \pm 32]_{3T}$	0.1196	−0.1168	4.0%
				$\sum = 198.1\%$
N1 - all	$[\pm 15, \pm 46]_{3T}$	3.6424	2.0994	100.0
N2 - all	$[\pm 15, \pm 46]_{3T}$	−0.1400	−1.0855	26.0
N3 - all	$[\pm 15, \pm 46]_{3T}$	0.0141	−0.0141	0.5
N4 - all	$[\pm 15, \pm 46]_{3T}$	1.0386	−0.7587	30.6
N5 - all	$[\pm 15, \pm 46]_{3T}$	0.1395	−0.1423	4.7
				$\sum = 161.8\%$

4.2. Laminates' failure load analysis

The laminates' failure load limits are determined by using the ME values for the dominating loads. For the fuselage scenario, the failure load is determined to

$$N5_{failure} = \frac{N5}{0.955} = \begin{bmatrix} -0.105 \\ 1.047 \\ 0.209 \end{bmatrix} \text{MN/m} \quad , \tag{17}$$

leading to a corresponding laminate stress of

$$\sigma_{failure} = \frac{N5_{failure}}{4 \cdot 8 \cdot 0.125 \text{ mm}} = \begin{bmatrix} -26.25 \\ 261.75 \\ 52.25 \end{bmatrix} \text{MPa} \tag{18}$$

and a corresponding strain of

$$\varepsilon_{failure} = [A^*]^{-1} \cdot \sigma_{failure} = \begin{bmatrix} -1.405 \\ 3.139 \\ 2.878 \end{bmatrix} 10^{-3} \quad . \tag{19}$$

The principle strains (in Microstrain) at failure are determined to

$$\varepsilon_{failure,I} = 3557, \quad \varepsilon_{failure,II} = -1822 \quad , \tag{20}$$

which is equivalent to the principle-strain magnitude (in microstrain) of

$$\sqrt{\varepsilon_{failure,I}^2 + \varepsilon_{failure,II}^2} = 3997 \quad . \tag{21}$$

Fig. 9 shows two additional results for the fuselage load set. In 9(a), Fig. 8(a) is re-plotted, while the full FPF envelope and the strength-parameter-based NC (radius 6053 microstrain) is added, to underline the determined laminate limits and the conservatism related to the used 4000 microstrain threshold.

Fig. 9(b) shows a result, which has been determined by considering the full 6053 microstrain NC radius within the optimization (see Table 4). While a 32-ply ($r = 8$) laminate was determined for the 4000 microstrain limit, a 24-ply laminate ($r = 6$) is identified for the updated strain limit, which is equivalent to 25% laminate-thickness reduction, which equals 25% weight saving.

When the data sets 'Best' are examined in the previous plots, the second objective of the optimization becomes obvious. It leads to the desired fact, that the best solution is identified from the sub-group belonging to the control load, while the solution with the minimum material effort is selected, in order to provide the highest load-increase capacity until failure occurs.

This procedure works fine as long the strain-magnitude levels for all examined load cases are within a rather narrow range. If a single-load is clearly dominating, it is recommended to re-analyze the group of feasible solutions thoroughly.

4.3. A direct approach to determine load-set specific minimum repeats

The previous analysis can be complemented by an analytical approach. The minimum number of repeats in a DD configuration to

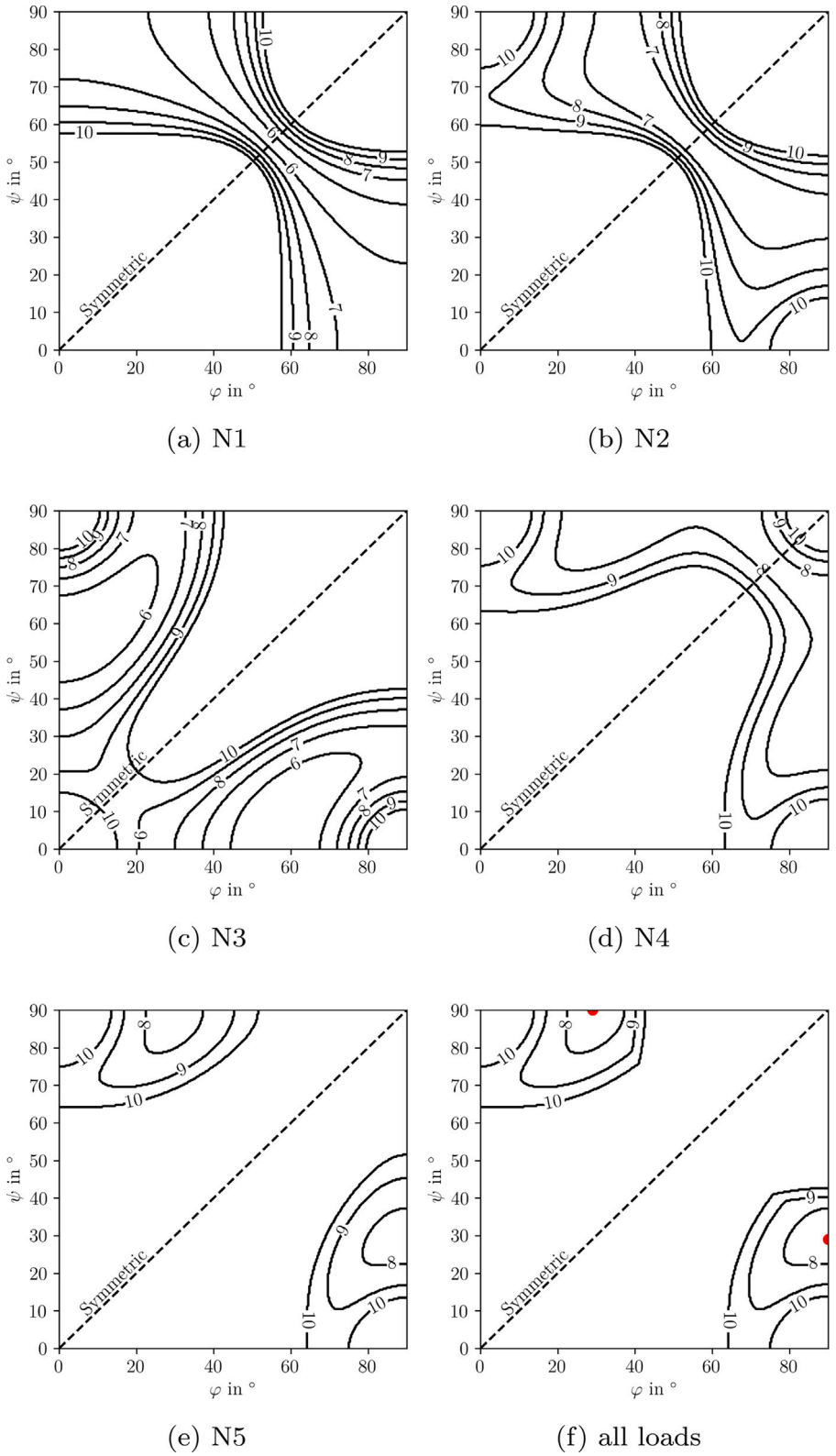

Fig. 10. R values for specific load cases. The red dot indicated the optimum solution $[\pm 90°, \pm 29°]$ from Fig. 8(a).

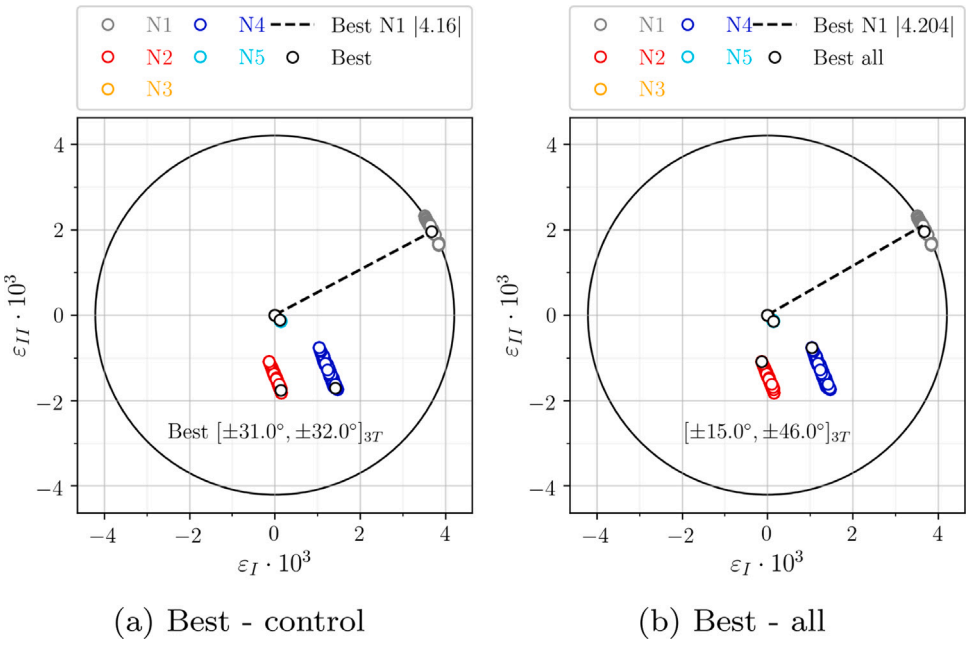

Fig. 11. Optimization results for two different approaches.

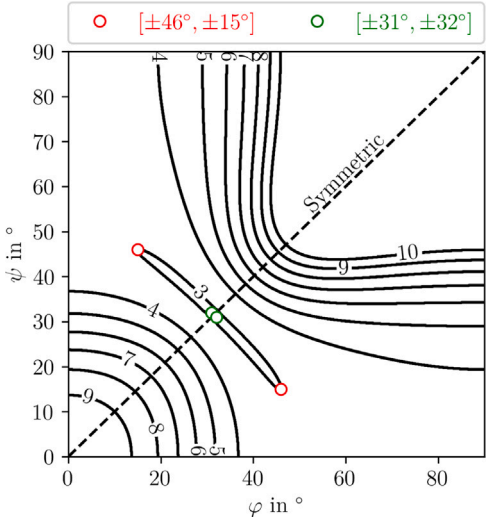

Fig. 12. Minimum repeats for Sprengholz et al. load case.

sustain a given load set can be determined analytically as well. The calculation basis on the defined ME (see Eq. (16)).

Whenever the ST is reached, the ME is equal to one, leading to

$$1 = \frac{\sqrt{2 \cdot \left(\frac{\varepsilon_x+\varepsilon_y}{2}\right)^2 + 2\left(\left(\frac{\varepsilon_x-\varepsilon_y}{2}\right)^2 + \left(\frac{\gamma_{xy}}{2}\right)^2\right)}}{ST} \quad , \tag{22}$$

which can be simplified to

$$ST^2 = \varepsilon_x^2 + \varepsilon_y^2 + \frac{\gamma_{xy}^2}{2} \quad . \tag{23}$$

Inserting strains from Eq. (15) into Eq. (23), and rearranging leads to the value for r, while $[a^*] = [A^*]^{-1}$, t_{ply} and N_x, N_y, N_{xy} are known from material data and load information.

$$r = \frac{\sqrt{\left(a_{11}N_x + a_{12}N_y\right)^2 + \left(a_{12}N_x + a_{22}N_y\right)^2 + \frac{a_{66}^2 N_{xy}^2}{2}}}{4 \cdot t_{ply} \cdot ST} \tag{24}$$

The determined r-value usually is of type float. Thus, it needs to be rounded to the next higher integer value using the ceil function $r \rightarrow \lceil r \rceil$, as only full building blocks are used with DD. Down rounding is not allowed in the present context, as it would lead to laminate overloads.

The described procedure can be applied to all conceivable ply-angle-orientation combinations of the DD building block, which allows for 2D illustration. For each ply-angle combination the minimum r-value is determined, leading to a continuous r-field. Due to the ceiling operation ($r \rightarrow \lceil r \rceil, ceil()$ function on Python) the plot shows different plateau levels.

Fig. 10 shows results for the fuselage load set, while Eq. (24) is applied for the each load of the examined set. Figs. 10(a)–10(e) show results for the individual loads. It can be seen that for selected loads (N1, N3) a minimum of 6 repeats is determined (24-ply laminate), a single load requires seven repeats (N2), while at least eight repeats are required for the loads N4 and N5.

As all loads of the load-set need to be sustained by the optimized laminate, the highest r-value of all load-specific minimum r-values is relevant. Fig. 10(f) shows a result, when all 5 loads are considered simultaneously. In fact, Eq. (24) is evaluated for all five loads, while the maximum determined r-value ($r = max(r_1, \ldots, r_5)$) is illustrated in the plot.

The comparison with Fig. 8(a) shows, that the identical DD laminate $[\pm 90, \pm 29]_{8T}$ is determined.

4.4. Discussion 'What is best?'

When load sets are examined usually a single load turns out being the control load. The procedure presented above is dominated by the control load case. Whenever, a single load is dominating, the optimized laminate solution will also be dominated/driven by it. However, when the best solution is affected by a dominating control load, it is not assured that the identified ply-angle optimum leads to the lowest MEs for the other load cases at the same time. In any case, it is assured that all strain-states fall within the Nettles circle. Thus, the defined laminates can sustain the examined load case. However, when all the feasible solutions are examined in detail, one can find solutions which show only slightly higher MEs for the control load, but significantly lower MEs for the other load cases.

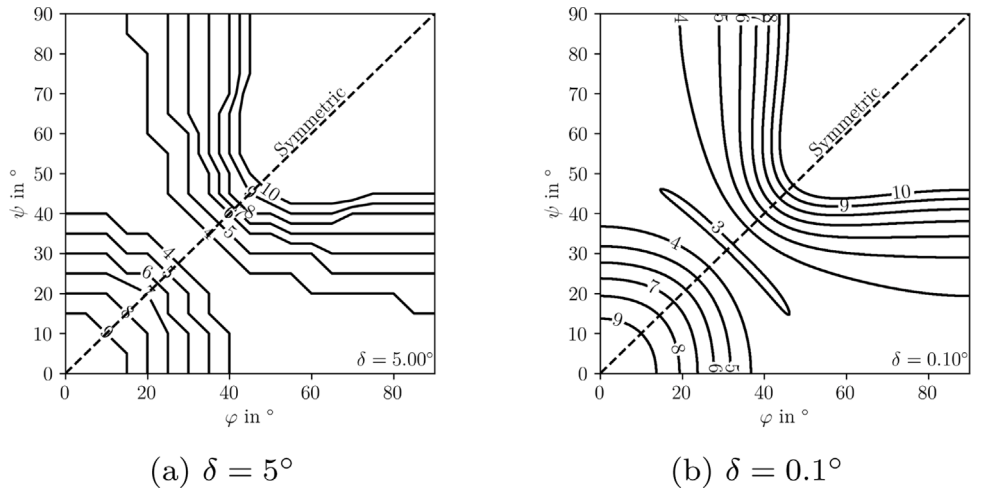

(a) $\delta = 5°$ (b) $\delta = 0.1°$

Fig. 13. Effect of design space resolution δ.

Sprengholz et al. [13] provide a data set to demonstrate the particular scenario. Table 7 provided the corresponding loads.

Sprengholz et al. analyzed the T300/976 material. The corresponding Engineering constants, strength data, the determined FPF envelope and the NC radius are provided above in Tables 2 and 3, Fig. 7(a) and Table 4, respectively.

Fig. 11(a) shows a result, which has been determined with the procedure presented in Section 4.1. In Sprengholz' load set N1 is clearly dominating. The determined best solution leads to a material effort of 98.9% for the N1 load (see Table 8). However, when MEs for the other loads are examined, the material efforts are among the highest for the load-specific groups, which is indicated by the large distances of the load-case specific-strain-stated from the NC's center. The dominance of the control load for the process becomes obvious. As all loads can be sustained and the control load can even be slightly increased, the solution in Fig. 11(a) is acceptable.

However, it can be shown, that other solutions in the group of all feasible solutions lead to lower summed MEs over all five load cases, while only a little ME increase is observed for the control load. The result, shown in Fig. 11(b), has been determined with a slightly modified procedure, which defines the best solution as the one with the lowest material effort over all load cases. A comparison of 'Best' and 'Best all' in Figured 11(a) and 11(b) shows the effect.

Table 8 provides the corresponding ME values for both runs. The control load focusses approach provides 1.1% load-increase capacity, while MEs are 16.1% and 22.1% higher for the loads N2 and N4, respectively.

The application of the updated procedure the MEs for N2 and N4 can be reduced drastically. The analytical procedure, presented in Section 4.3, allows for illustrating the different solutions. Both solutions are well on the $r = 3$ plateau, as shown in Fig. 12.

Finally, both solutions fulfill the requirement and it is/remains the task of the stress engineer to decide which approach is considered best. As long reliable strain-thresholds are used within the calculations, both strategies will lead to safe laminates.

4.5. A comment on design-space resolution

Eq. (24) allows for the direct determination of the best DD solution for a given load and also for load sets. It shall be highlighted that the design-space resolution plays an important role. From a manufacturing perspective, in an AFP context for example, full-degree ply angles are considered realistic, while angles with a single digit are considered the technical limit. Fig. 13 shows the effect of deviating δ steps for the r-plateau determination. Fig. 13(a) is created based on 361 configurations, while Fig. 13(b) represent 811801 DD configurations.

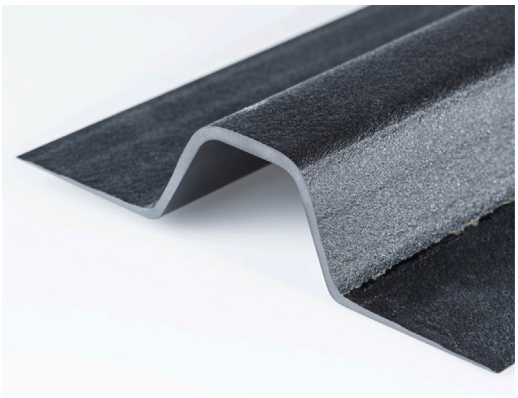

Fig. 14. Omega-stringer application: Unique DD tapering feature allows for peel-stress reduction and weight saving.

5. Conclusion

The present paper demonstrates how unique design features of the Double–Double (DD) family of laminates can be beneficially used to identify best laminates for given load sets, while the term 'best' is understood as a laminate which shows the lowest material effort within the group of lightest laminates. The examined DD laminates are described by $[\pm\varphi, \pm\psi]_{rT}$. They are always balanced but asymmetric, while it can be shown that detrimental asymmetry effects, such as warpage and bending–twist coupling diminish proportional with $1/r$, $1/r^2$, respectively, allowing for making accurate parts, which in fact are asymmetric. In the failure assessment context, the omni first-ply-failure (FPF) envelopes in strain space have been adopted in the presented procedure, as those allow for assessing failure on laminate level instead of the rather laborious ply-wise strategies. The FPF envelopes are further simplified by a transfer to principal-strain space. This basically reduces the number of relevant strain parameters and allows for defining the Nettles-circle failure envelope, which is a simplification of the unit-circle-failure envelope. Meaningful 2D graphical illustrations become possible, due to the simplifications, which allow for illustrating the executed optimization process.

The proposed optimization scheme is presented for three different load sets, each consisting of five individual loads. The scheme determines the optimum ply-angle combination φ, ψ and the minimum

number of repeats r, which leads to the lightest laminates within the design space. It is demonstrated that the optimization can be executed using strength-data-based NCs or a self-defined design-strain-magnitude threshold, as for example 4000 microstrain.

Due to the unique DD-layup features complex stacking-permutation discussions do not impede the optimization procedure. The established combination of NC with the DD approach allows for the direct determination of a 'best' laminate for a given load set, while the optimization approach assures that the selected strain threshold is not violated.

The graphical illustrations are found a powerful support for stress engineers. They allow for visualizing the optimization process, its results and they ease the identification of the dominant/control load within a load set. It is also demonstrated in this paper that the NC/DD combination allows for an analytical determination of the minimum number of repeats over the full DD design space, which can even be executed without optimization. Thus, the group of feasible DD laminates for a given load set can be directly visualized in a single plot.

5.1. Outlook

In upcoming studies, the outlined DD-specific advantages in laminate optimization will be accompanied by experimental investigations. The DD-concept, in combination with today's (automated) manufacturing techniques, such as single-sided diaphragm forming, promises significant weight-reduction potential and automation potential, which needs to be proven. Fig. 14 shows an omega-stringer example, which demonstrates the unique tapering capabilities of DD laminates around the stringer feet, which reduce peel-stress issues and save weight. The stringer has been made by the author from conventional low-grade prepreg by using the card-sliding approach outlined in [3].

The realized DD laminate combines a quasi-isotropic base laminate with a more orthotropic stacking around the middle-chord in a single $[\pm 19.3, \pm 67]_{1-8T}$ laminate, varying from a single building-block at the outer feet ends to eight repeats at the middle-chord area.

CRediT authorship contribution statement

Erik Kappel: Sole author, Responsible for everything leading to the paper.

Acknowledgments

The author particularly thanks Professor Steve Tsai for the intensive exchange, many valuable discussions on DD and beyond, and also for providing Stanford's Composites Workshop in 2021.

The author particularly thanks Dr. Alan Nettles and Dr. Will Guin for their critical reviews and the valuable comments, which clearly helped to improve the paper. The author acknowledges valuable reviews from Prof. Klaus Rohwer, Yannick Boose. The research leading to these results has received funding from the German Federal Ministry for Economic Affairs and Energy (BMWI) under project numbers 20A2103C (MuStHaF-DLR) and 20W1729C (MoveIntegR).

Declaration of competing interest

The author declares that he has no known competing financial interests or personal relationships that could have appeared to influence the work reported in this paper.

References

[1] S.W. Tsai, J.D.D. Melo, Composite Materials Design and Testing - Unlocking Mystery with Invariants, Stanford University, 2015.
[2] S.W. Tsai, J.D.D. Melo, S. Sihn, A. Arteiro, R. Reinsberger, Composite laminates - theory and practice of analysis, design and automated layup, stanford, 2017.
[3] S.W. Tsai, Double-double: New family of composite laminates, AIAA J. (2021) http://dx.doi.org/10.2514/1.J060659.
[4] S.W. Tsai, et al., Composite double-double and grid/skin structures, in: Low Weight/Low Cost Design and Manufacturing, Stanford University, 2019.
[5] A. Riccio, F. Di Caprio, Double-double for aircraft structures. DD workshop 2021 - July 20th, 2021.
[6] A.T. Nettles, Basic Mechanics of Laminated Composite Plates - NASA Reference Publication 1351, Technical report, NASA, 1994.
[7] S.W. Tsai, J.D.D. Melo, A unit circle failure criterion for carbon fiber reinforced polymer composites, Compos. Sci. Technol. 123 (2016) 71–78.
[8] A. Baker, S. Dutton, D. Kelly, Composite Materials for Aircraft Structures, second ed., in: AIAA Education Series, 2004, p. 465.
[9] M.A. Caminero, G.P. Rodríguez, V. Muñoz, Effect of stacking sequence on charpy impact and flexural damage behaviour of composite laminates, Compos. Struct. (2015).
[10] E. Calik, N. Ersoy, F. Oz, Experimental and numerical progressive failure analysis of corrugated core type composite sandwich structure, in: ECCM18-18th European Conference on Composite Materials Athens, Greece, 2018.
[11] Llobet, et al., Progressive matrix cracking in carbon/epoxy cross-ply laminates under static and fatigue loading, Int. J. Fatigue 119 (2019) 330–337.
[12] K.V. Williams, R. Vaziri, Application of a damage mechanics model for predicting the impact response of composite materials, Int. J. Comput. Struct. 79 (2001) 997–1011.
[13] M. Sprengholz, H. Traub, M. Sinapius, S. Dähne, C. Hühne, Rapid transformation of lamination parameters into stacking sequences, Compos. Struct. 276 (2021) 114514.
[14] S.W. Tsai, et al., LamSearch Tool - the Composites Design Workshop XXI, Stanford University, 2021, pp. 19–23, July.
[15] M. Schlueter, S. Erb, M. Gerdts, S. Kemble, J.J. Rückmann, MIDACO on MINLP Space Applications Advances in Space Research, Elsevier, 2013, 51, 7, 1116 1131.